Applied Catalysis B: Environmental 206 (2017) 479–489

Contents lists available at ScienceDirect

Applied Catalysis B: Environmental

journal homepage: www.elsevier.com/locate/apcatb

An alternative to in situ photocatalytic degradation of microcystin-LR by worm-like N, P co-doped TiO_2/expanded graphite by carbon layer (NPT-EGC) floating composites

Xin Wang[a,b], Xuejiang Wang[a,*], Jianfu Zhao[a], Jingke Song[a], Lijie Zhou[c], Jiayi Wang[a], Xin Tong[b], Yongsheng Chen[b,*]

[a] College of Environmental Science and Engineering, State Key Laboratory of Pollution Control and Resource Reuse, Tongji University, Shanghai 200092, China
[b] School of Civil and Environmental Engineering, Georgia Institute of Technology, Atlanta 30332, USA
[c] Shenzhen Academy of Environmental Sciences, Shenzhen 518001, China

ARTICLE INFO

Article history:
Received 16 October 2016
Received in revised form 10 January 2017
Accepted 18 January 2017
Available online 20 January 2017

Keywords:
Floating photocatalyst
TiO_2
Expanded graphite
Adsorption
MC-LR

ABSTRACT

In recent years, harmful algal blooms (HABs) frequently occur in eutrophic lakes all over the world. It causes the accumulation of microcystin-LR (MC-LR) in water, thus giving a great threat to aquatic animals and human beings. In this paper, a facile sol-carbonization method was used to synthesize N, P co-doped TiO_2/expanded graphite by carbon layer (NPT-EGC) floating photocatalysts, which are designed for in situ photocatalytic degradation of MC-LR. XRD, N_2 adsorption/desorption, FESEM/EDS, TEM, FTIR, XPS, UV–vis DRS and the PL spectrum were used to investigate the physicochemical and photoelectricity properties of the NPT-EGC photocatalysts. The results showed that NPT-EGC has a worm-like structure with N, P co-doped TiO_2 particles distributed on the surface. The calcination temperatures have influences on the forming of TiO_2 and carbon layer, specific surface area and photocatalytic activity. Among the different NPT-EGC photocatalysts, the photocatalyst calcined at 450 °C (NPT-EGC450) exhibited the strongest photo-absorption and the lowest recombination rate of photo-generated charge carrier. As a result, NPT-EGC450 achieved the highest removal rate of MC-LR (99.4%) following 9 h of irradiation, which is mostly attributed to photocatalytic degradation. LC–MS analysis showed most MC-LR molecules have been mineralized into small molecules. After three consecutive cycles, the NPT-EGC floating photocatalyst exhibited excellent reusability and stability, which indicates the floating photocatalysis is a promising technique for MC-LR degradation in the future.

1. Introduction

Occurrences of harmful algal blooms (HABs) in eutrophic waters are a growing threat worldwide. Microcystins (MCs) are a group of cyanotoxins generated by harmful algae such as *Microcystis aeruginosa* [1]. Among all known MCs, microcystin-LR (MC-LR) is the only one that has been given a guideline value of 1 μg/L in drinking water [2]. It is a heptapeptide cyclic compound (see Scheme 1) with an Adda (hydrophobic amino acid) group, containing leucine (L) and arginine (R) in variable positions [3]. Harmful algal cells produce and retain MC-LR until they are ruptured, at which point the toxin will be released into the surrounding aquatic environment [4]. MC-LR molecule is very stable due to its cyclic structure and the presence of the unique amino acids, which can resist thermal and hydrolytic degradation; hence, it cannot be removed by common chemical treatments [5].

Titanium dioxide (TiO_2) has been intensively studied and has proven to be a highly useful and active photocatalyst to remove or degrade recalcitrant organic contaminants for water purification. In 1999, Lawton et al. found that the TiO_2 photocatalysis process can destroy some MC-LR groups and significantly reduce the toxicity [6]. Considering the economic factors, more and more researchers want to apply TiO_2 photocatalysis to the in situ remediation of MC-LR polluted eutrophic waters using solar light as the light source [7–10]. However, TiO_2 can only utilize the light with wavelengths shorter than 385 nm (UV range) due to its wide band gap (e.g., Eg ≈ 3.2 eV for anatase), which limits its application with solar light [11]. Dionysiou's group has made many efforts to improve

* Corresponding authors.
E-mail addresses: wangxj@tongji.edu.cn (X. Wang), yongsheng.chen@ce.gatech.edu (Y. Chen).

http://dx.doi.org/10.1016/j.apcatb.2017.01.046
0926-3373/

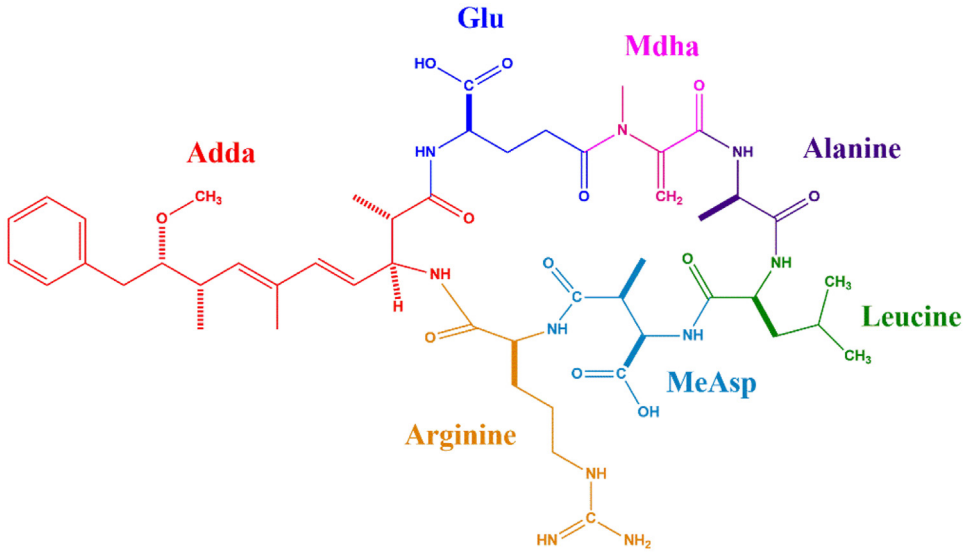

Scheme 1. Structure of microcystin-LR.

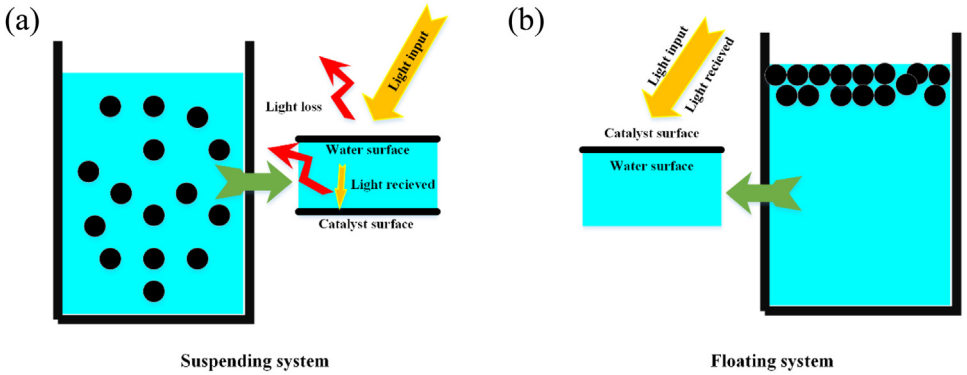

Scheme 2. Light energy transmission in (a) suspending system and (b) floating system.

the efficiency of photocatalytic degradation of MC-LR under visible light irradiation by an ion doping technique [2,4,5,12–16]. However, practically, it's a keypoint to ensure that the photocatalyst can receive sufficient light energy to trigger the reaction. As a result, the design of photocatalytic system is of great importance. For most of the photocatalytic treatments, the photocatalysts are kept in a suspending system by mechanical agitation as a result of the heavy weight of whether the powder photocatalysts or the immobilized photocatalysts. This results in a lot energy loss through light reflection and water absorption during the optical transmission (see Scheme 2a). In consideration of the low energy utilization in the suspending system, floating photocatalysis system has drawn more and more attention since it can take in light energy directly (see Scheme 2b). In addition, the floating property makes the catalysts recycling more convenient, which can lower the environmental risk after the photocatalytic treatments [17]. In floating photocatalysis system, the catalysts achieve the floating property by immobilized on the light weight substrate such as vermiculite, expanded polystyrene and cenosphere [18–20]. In our previous studies, we found expanded graphite (EG) has excellent porous structure and can float on the surface of water permanently, which is considered as a remarkable catalyst carrier compared with the conventional floating carriers. However, considering the mechanical strength of EG is not strong enough, it still need to be enhanced. On the other hand, the former investigated photocatalytic process of MC-LR degradation was considered too simple. When used as in situ treatment, photocatalysis would face the challenges from environmental coexisting substances in eutrophic waters such as natural organic matter (NOM), dead algal cells, cytochromes and inorganic ions. To our knowledge, the influences of these substances were rarely involved in previous studies.

In this study, we developed a novel floating photocatalyst, namely, N, P co-doped TiO_2/expanded graphite by carbon layer (NPT-EGC) composites. Sucrose was used to form a carbon layer on the surface of expanded graphite to enhance the mechanical strength while N, P co-doped TiO_2 particles were immobilized on the surface of the enhanced expanded graphite as the photocatalytic active sites. This hybrid material can float on the surface of water as a result of the light weight and porous structure. This design can make the photocatalysts maximally utilize the light energy and easy to recycle. The NPT-EGC photocatalysts were characterized by XRD, N_2 adsorption/desorption, FESEM/EDS, TEM, FTIR, XPS, UV–vis DRS and the PL spectrum. The adsorption and photocatalysis behavior of MC-LR by NPT-EGC were investigated. The byproducts generated during the photocatalytic degradation were also analyzed by LC–MS. Furthermore, the environmental coexisting substances were taken into consideration in the photocatalytic process, which is providing guidance to in situ application in eutrophic waters.

2. Materials and methods

2.1. Preparation of NPT-EGC floating photocatalysts

Five mL tetrabutyl titanate, 10 mL anhydrous ethanol and 5 mL acetylacetone were dissolved completely to obtain Solution A. The dopants (0.5 g urea and 1 mL phosphoric acid) were dissolved into the mixture of 5 mL anhydrous ethanol, 5 mL acetylacetone and 100 mL distilled water, while adjusting the pH value to 2.5 with hydrochloric acid to form Solution B. Solution A was added into Solution B slowly with stirring. After that, the mixture was stirred for 1 h and ultrasonic dispersion took place for 30 min to obtain TiO_2 yellow sol.

Three grams of EG, which was pretreated with soaking into 40 wt% sucrose solution for 1 h, was added into the prepared TiO_2 sol with stirring for 30 min. After that, the mixture was aged for 5 h. The EG was then taken out and dried at 105 °C to get the precursor of NPT-EGC. The precursor was calcined at 350, 450, 550 and 650 °C for 3 h with N_2 protecting the environment to obtain the final NPT-EGCX (X stands for the calcination temperature).

2.2. Characterization

X-ray diffraction (XRD, Bruker D8 ADVANCE) was performed with an X-ray diffractometer using Cu Kα radiation to analyze the crystal structure. The specific surface areas were measured using N_2 adsorption/desorption isotherms according to the Brunauer-Emmett-Teller analysis (BET, Micromeritics, ASAP 2020). The morphology and structure were observed using field-emission scanning electron microscopy (FESEM, Zeiss Ultra55) together with an energy dispersion spectrometer (EDS) and transmission electron microscope (TEM, Tecnai G2, FEI). The IR spectrum was recorded as KBr pellets at room temperature on a fourier transform infrared spectroscopy (FTIR, Nicolet Instrument Corporation, USA). X-ray photoelectron spectroscopy (XPS, Thermo-VG Scientific ESCALAB 250) was performed to determine the elemental composition and electronic structure. UV–vis diffuse reflectance spectra (UV-vis DRS, Shimadzu UV-2550) were measured in the range 200–800 nm using $BaSO_4$ as a reference to investigate the light absorption features. PL spectra were recorded by QM40 combined fluorescence lifetime and steady state spectrometer using a 450 W Xenon lamp as the excitation light source.

2.3. Photocatalytic experiments

The photocatalytic degradation of MC-LR was conducted in the DY-F photochemical reactor (Shanghai Deyangyibang Instruments Co., Ltd. China). The reactor was equipped with several accessories, such as a magnetic force stirrer, quartz reaction tube, and a condensation tube, which can keep the reaction temperature steady and prevent the evaporation of water. The Xenon lamp (XE-JY500, 500 W) with a UV cut off filter (1 M sodium nitrite solution, $\lambda > 385$ nm) was used as a visible light source and it was maintained in the center of the glass vessels. The light intensity of the solar spectrum was measured to be ca. 2 mW/cm^2. The initial concentration of MC-LR was 2 mg/L and the obtained photocatalyst was added at the ratio of 2 g/L. At a predetermined time of 1 h intervals (1–9 h) after turning on the light, 0.2 mL samples were taken out and filtered with 0.22 μm aqueous phase syringeless filters. The concentration of MC-LR was quantified using a high performance liquid chromatograph (HPLC, Shimadzu LC-20A) with a photodiode-array detector (PDA) set at 238 nm and an Agilent ZORBAX Eclipse Plus C18 column (250 mm × 4.6 mm × 5 μm). The mobile phase was water containing 0.05% TFA (v/v) and methanol, and the ratio was 35:65. The injection volume of the sample was 20 μL and the flow rate was 0.6 mL/min. A LC–MS instrument (Dionex, UltiMate 3000 for LC and Bruker, MicroTOF11 for MS analysis) was used to monitor the reaction intermediates by full scanning from m/z 300–1150 in the positive ion mode. A trap software workstation was used for the LC–MS instrument control and data analysis. The mobile phase was a gradient elution of formic acid (pH = 2.6) and acetonitrile. Gradient elution was programmed as 0–20% acetonitrile (10 min) followed by an increase to 35% (10 min), 60% (15 min), and 80% (10 min) [21].

3. Results and discussion

3.1. Characterization

The crystalline phases of the NPT-EGC photocatalysts and EG reference were determined by XRD (Fig. 1a). Compared with EG, no new diffraction peaks are observed in NPT-EGC photocatalysts with different calcination temperatures. Apparently, the NPT-EGC composites maintained the basic structure of the EG substrate. As for the phase structure of TiO_2 particles in the floating photocatalysts, it may be covered by the strong diffraction peaks of graphite or formed amorphous state. In order to ensure the phase structure of TiO_2, N, P co-doped TiO_2 (NPT) photocatalysts were synthesized according to the preparation method of NPT-EGC in the absence of EG and sucrose. The XRD patterns of NPT photocatalysts are shown in Fig. 1b. It has been observed that there are two diffraction peaks at 20.0° and 26.4° for NPT350. The peak at 20.0° is attributed to TiO_2 with O defects (JCPDS 40-0806) while the peak at 26.4° corresponds to the combination of graphite-2H (JCPDS 41-1487) and O deficient TiO_2. With the increase of calcination temperature, the amount of C in NPT photocatalysts decreased. At the same time, some impure TiO_2 crystal planes between 20.0° and 26.4° emerged. This resulted in the intensity decrease of the peak at 26.4° and the combination of the two peaks into one broad peak. The N_2 adsorption/desorption isotherms of NPT-EGC and EG reference are shown in Fig. 2. It has been found that N_2 adsorption volumes decreased after a carbon layer and TiO_2 particles were immobilized on the surface of EG. The specific surface area of EG, NPT-EGC350, NPT-EGC450, NPT-EGC550 and NPT-EGC650 were calculated to be 67.33 m^2/g, 29.94 m^2/g, 39.39 m^2/g, 24.78 m^2/g and 31.79 m^2/g, respectively. It can be seen that the specific surface areas of the as-synthesized NPT-EGC hybrid catalysts have decreased to some extent after modified with carbon layer and TiO_2 particles comapred with the bare EG substrate.

The morphology and microstructure of NPT-EGC450 was characterized by FESEM/EDS and TEM analysis as shown in Figs. 3 and 4. Fig. 3a shows that the as-prepared NPT-EGC floating photocatalyst worm-like structure with a lot of wrinkles on the surface, which is due to the EG substrate (see Fig. S1). The magnifying graph shows TiO_2 particles distributed on the surface of EGC (Fig. 3b). The EDS mapping shows the NPT-EGC450 floating photocatalyst containing C, Ti, O, N and P elements with a content of 82.59, 1.97, 12.86, 1.68 and 0.90 wt%, respectively (Fig. 3c–g). The EDS mapping of Ti shows TiO_2 particles have a wide distribution on the carbon phase, and the TiO_2 coverage is more easily formed on the surface of wrinkles. The TEM images are shown in Fig. 4. The micrograph clearly presents the laminar morphology of EG substrate with TiO_2 particles modified on the surface.

The surface functional groups of NPT-EGC were confirmed by FT-IR spectra. From Fig. 5, the strong bands at 3483 cm^{-1}, 3684 cm^{-1} and 1642 cm^{-1} are attributed to the O—H bending modes of adsorbed water molecules [22,23]. There were two weak bands at 1385 cm^{-1} and 1041 cm^{-1}. The former corresponds to the stretching of the N—O group, while the latter is assigned to the stretching of the P—O group [24]. The band at 400–800 cm^{-1} is attributed to Ti—O stretching and Ti—O—Ti bridging stretching modes [22]. With the increase of calcination temperature, the N—O and P—O bands

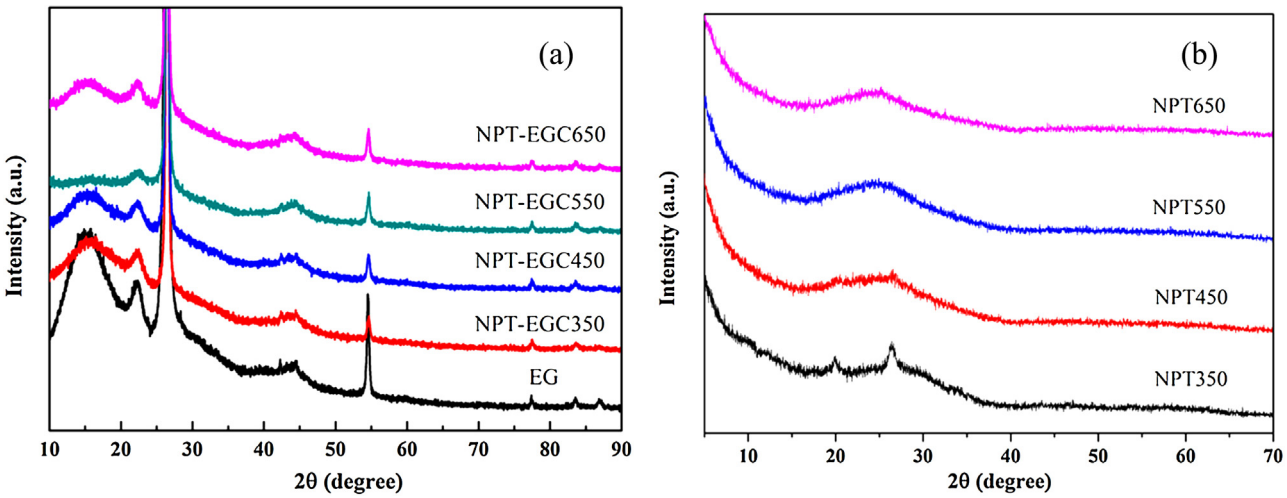

Fig. 1. XRD pattern of (a) NPT-EGC and (b) NPT catalysts.

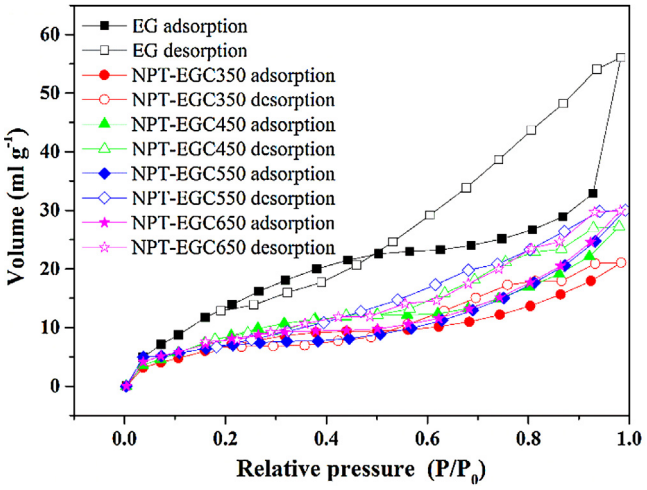

Fig. 2. N_2 adsorption-desorption isotherms of EG and NPT-EGC.

disappeared with the loss of dopants; meanwhile, the Ti—O band became sharper for the crystal growth.

XPS was used to further determine the chemical states of the constituent elements (Fig. 6). As shown in Fig. 6a, the NPT-EGC floating photocatalysts predominantly contain C, Ti, O, N, and P, which is in agreement with EDS results. It clearly proves that N and P elements have successfully doped into TiO_2. The high resolution Ti 2p XPS spectrum of NPT-EGC450 is shown in Fig. 6b. It is reported that 458.1 eV is the binding energy of Ti $2p_{3/2}$ for pure TiO_2 [25]. Fig. 6b shows Ti $2p_{3/2}$ and Ti $2p_{1/2}$ of NPT-EGC450 with an obvious chemical shifts appearing at 460.8 eV and 466.8 eV, which gives direct evidence of the occurrence of oxygen vacancies caused by N and P doping. Because oxygen is a highly electronegative element, oxygen vacancies can withdraw the electron density from Ti. As a result, the binding energy of Ti in NPT-EGC increases with the increase of oxygen vacancy concentration [26]. The high resolution N 1s and P 2p XPS spectra are shown in Fig. 6c and d. Fig. 6c shows a broad peak between 398 and 406 eV, which stands for the characteristic of N doping. Three peaks are discovered by fitting the curves. The peak at 400.2 eV is assigned to substitutional N for O in the form of O—Ti—N bonding. The peak at 401.5 eV indicates the surface adsorption of N_2. The peak at 402.9 eV should be related to nitrogen species bound to various surface oxygen sites [27]. From Fig. 6d, the P 2p binding energy is observed at 134.2 eV, suggesting that P in the floating photocatalyst exists in a pentavalent-oxidation state (P^{5+}). No peak belonging to P^{3-} (128.6 eV) is observed, indicating the absence of Ti-P bonds [24].

The UV–vis DRS and PL spectra were performed in order to further investigate the effect of calcination temperature on the photoelectric characteristics of NPT-EGC using P25 and EG as the references. The UV–vis DRS results are shown in Fig. S2 with the finding of a strong absorption in the visible light region for EG. NPT-EGC photocatalysts present similar curves to EG, but their absorption intensities are much stronger than EG and P25 catalyst powder. For the influence of carbonic substrate on light absorption, the bandgap energy (Eg) of the floating photocatalysts cannot be calculated using traditional methods. However, it can be verified that NPT-EGC450 has a higher photo-absorption than the other NPT-EGC photocatalysts. PL analysis was performed to investigate the separation efficiency of photogenerated electrons and holes in these hybrid materials. Fig. S3 shows the PL spectra of NPT-EGC photocatalysts and P25 powder excited at 385 nm. The PL spectra present the similar position of emission peaks, which are centered at about 460 nm and 550 nm. However, compared with P25, the emission intensities of NPT-EGC photocatalysts have significantly decreased, especially for NPT-EGC450, which indicates that NPT-EGC450 floating photocatalyst has a much lower recombination rate for a photo-generated charge carrier [28]. That is to say, the recombination of photogenerated charge carriers is greatly inhibited by the successful doping of N and P at the calcination temperature of 450 °C.

3.2. Photocatalytic degradation of MC-LR by NPT-EGC

Generally, the photocatalytic degradation is considered as a surface-catalyzed reaction that will take place on the pollutant-adsorbed sites over photocatalysts [29]. The surface adsorption enriches the pollutant molecules on the substrate, which is especially important to low concentration pollutants. The adsorption process causes the concentration effect in chemical reactions, thus enhancing photocatalytic activity. Xue et al. found that the photocatalytic reactions degrade pollutant molecules, and thereby enhance pollutant adsorption on the surface of the photocatalyst [30], while Xiong et al. reported too high adsorption would inhibit the photocatalytic degradation [31]. Therefore, the adsorption onto NPT-EGC photocatalyst is of great importance for the study of photocatalytic degradation activity. The adsorption capacity by 2 g/L NPT-EGC photocatalysts with the initial concentration of 2 mg/L

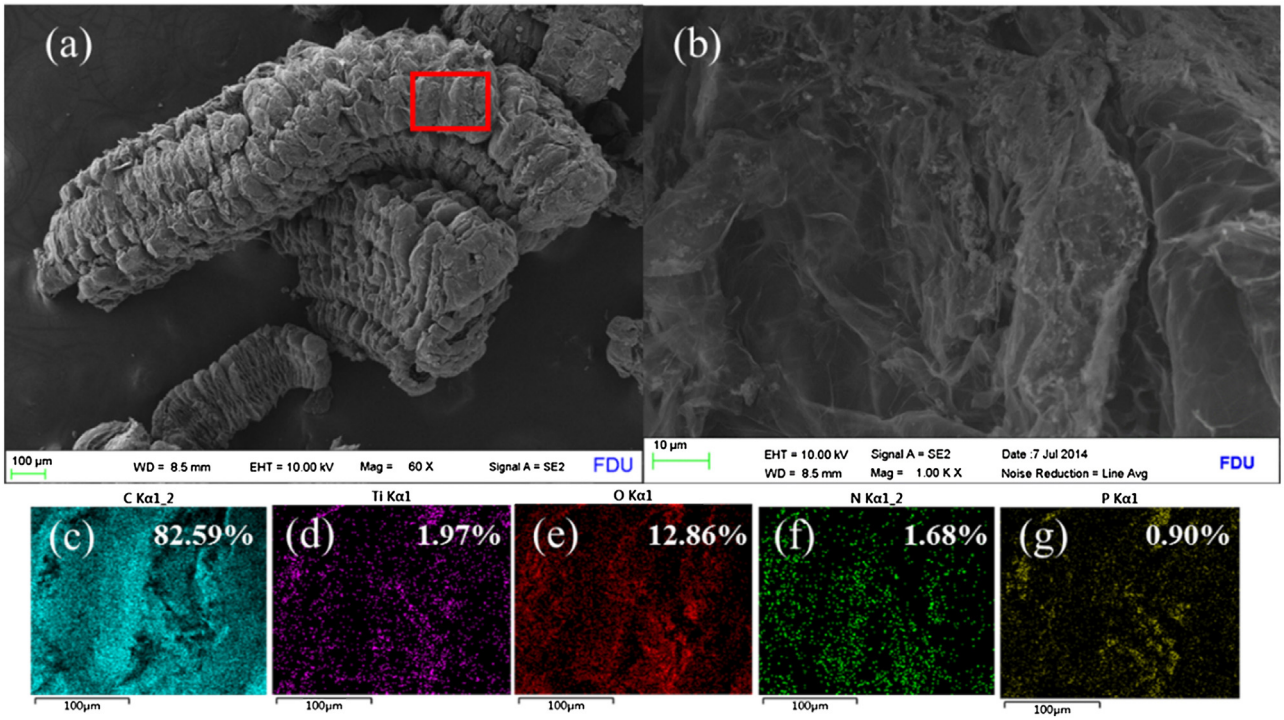

Fig. 3. SEM and EDS-mapping images of NPT-EGC450: (a) A low magnification image, (b) a high magnification SEM image, (c) mapping of C, (d) mapping of Ti, (e) mapping of O, (f) mapping of N, and (g) mapping of P.

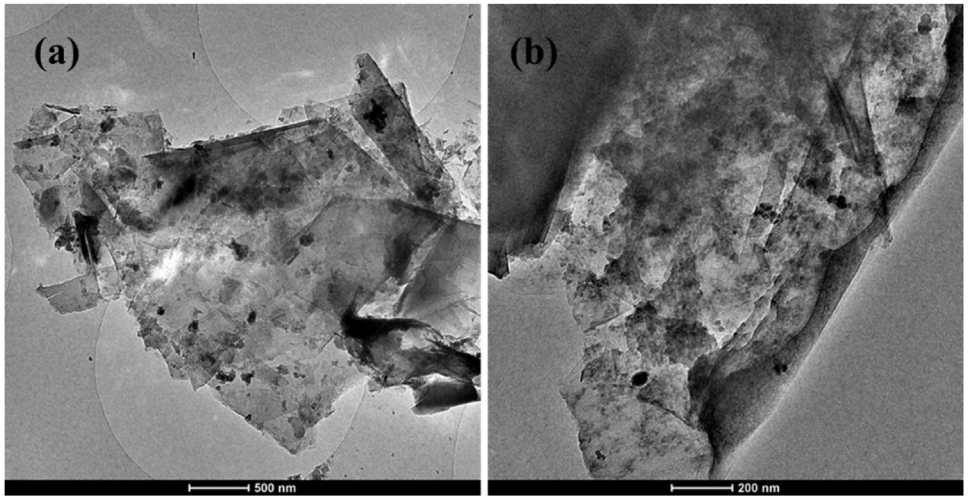

Fig. 4. TEM images of NPT-EGC450.

MC-LR is displayed in Fig. S4. The adsorbed quantities of MC-LR at time t, q_t (mg/g), are calculated according to Eq. (1):

$$q_t = \frac{(C_0 - C_t)V_0}{w_c} \quad (1)$$

where C_0 and C_t (mg/L) are the initial concentration and concentration at time t, respectively; V_0 is the volume of MC-LR solution (L), and w_c is the mass of catalyst (g). Both the pseudo-first-order (Eq. (2)) and pseudo-second-order (Eq. (3)) Lagergren kinetic modes are used to estimate the equilibrium adsorption capacity (q_e) and adsorption rate constant (k). The correct values are chosen based on the higher correlation coefficient r^2.

$$\log(q_e - q_t) = \log q_e - \frac{k_1 t}{2.303} \quad (2)$$

$$\frac{t}{q_t} = \frac{1}{k_2 q_e^2} + \frac{t}{q_e} \quad (3)$$

where q_e and q_t are the adsorption capacity at equilibrium and at time t, respectively (mg/g). Meanwhile, k_1 (1/min) and k_2 (g/(mg min)) are the rate constant of the pseudo-first-order and pseudo-second-order sorption, respectively [32].

The fitted parameters to the Lagergren equation are presented in Table 1. In the present study, the pseudo-first-order adsorption kinetics is adopted based on the higher r^2 values of 0.98650–0.99301. This result indicates that the adsorption of MC-LR is controlled by diffusion or mass transfer inside the substrate. The q_e and k_1 values were determined from the fitting equations. The adsorptive capacity of MC-LR is closely related to the specific surface area results, and NPT-EGC450 exhibited the best adsorp-

Table 1
Adsorption and photocatalytic degradation kinetic parameters of NPT-EGC.

Samples	Lagergren pseudo-first-order			Lagergren pseudo-second-order			Langmuir-Hinshelwood	
	q_e (mg/g)	k_1 (min^{-1})[a]	r^2	q_e (mg/g)	k_2 (g/mg min)[b]	r^2	k_{app} (h^{-1})[c]	r^2
NPT-EGC350	0.1267	0.01112	0.99000	0.2091	0.0310	0.88358	0.11984	0.99182
NPT-EGC450	0.4911	0.02392	0.98650	0.6532	0.0287	0.94207	0.58651	0.99408
NPT-EGC550	0.2256	0.02038	0.99301	0.3316	0.0384	0.92017	0.28999	0.99781
NPT-EGC650	0.4326	0.01223	0.98835	0.5959	0.0168	0.89973	0.36272	0.98935

[a] Equilibrium adsorption capacity and pseudo-first-order adsorption rate constant, determined from parameters of the plot of $q_t = f(t)$.
[b] Equilibrium adsorption capacity and pseudo-second-order adsorption rate constant, determined from the slope and intercept of the plot of $(t/q_t) = f(t)$.
[c] Apparent first-order degradation rate constant, evaluated from the slope of the plot of $-\ln(C/C_0) = k_{app}t$.

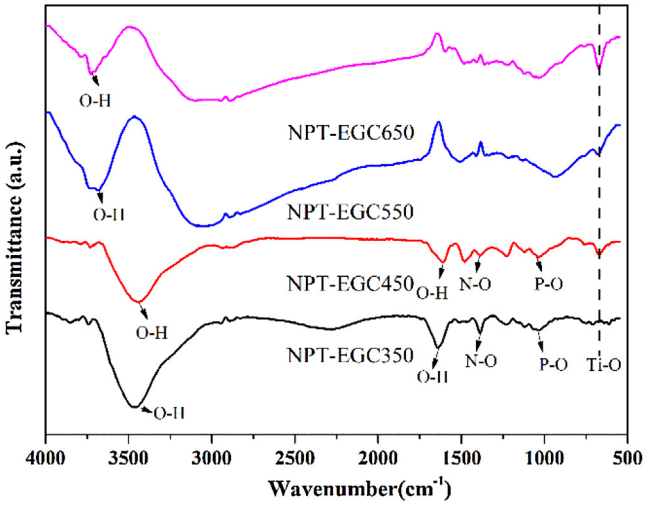

Fig. 5. FT-IR spectra of NPT-EGC.

tivity, ca. 0.4911 mg/g, along with the highest k_1 value of about 0.02392 min^{-1}.

The comparison of photocatalytic activities of different NPT-EGC photocatalysts for MC-LR degradation under visible light irradiation is shown in Fig. 7. It can be seen that MC-LR molecules are stable and can hardly be directly photo-degraded under visible light irradiation. Among the NPT-EGC photocatalysts with different calcination temperatures, NPT-EGC450 presents the highest removal of MC-LR (99.4%) following 9 h irradiation. Compared with previous studies, the removal results are considered at a high level (see Table S1). The photocatalytic degradation kinetics of MC-LRwith NPT-EGC photocatalysts were evaluated by fitting the experimental data to the Langmuir-Hinshelwood (L-H) model. The pseudo-first-order kinetics equation (Eq. (4)) was used as follows [17]:

$$-\ln\left(\frac{C_t}{C_0}\right) = k_{app}t \quad (4)$$

where C_0 and C_t are the reactant concentration at $t = 0$ and t, respectively, and k_{app} (h^{-1}) is the apparent reaction rate constant determined by plotting $-\ln(C/C_0)$ vs. the reaction time (t).

Fig. 7b shows the kinetic studies of different NPT-EGC photocatalysts and the calculated parameters are listed in Table 1. The apparent first-order degradation rate constant (k_{app}) of NPT-EGC350, NPT-EGC450, NPT-EGC550 and NPT-EGC650 can be calculated as 0.11984, 0.58651, 0.28999 and 0.36272 h^{-1}, respectively. The results show that NPT-EGC450 has the highest photocatalytic activity for MC-LR degradation under visible light irradiation. In order to confirm the contributions of adsorption and photocatalytic degradation to the final removal of MC-LR, the NPT-EGC photocatalysts were taken out after photocatalytic experiments and desorbed in 0.1 N NaOH [33]. The MC-LR concentration in the desorbed solution is treated as the adsorption part in the final removal. The distributions of the adsorption part and the photocatalytic degradation part in final removal of MC-LR are shown in Fig. 8, where most removal of MC-LR is due to the photocatalytic degradation. NPT-EGC450 photocatalytically degraded the most adsorbed MC-LR and achieved the highest photocatalysis contribution (99.5%) and the lowest adsorption contribution (0.5%) to the final removal of MC-LR. This result is expectedly due to the synergistic effect of adsorption and photocatalytic degradation. Moreover, it suggests the photocatalyst has the ability of continuous purification, which is of great importance in practical application.

3.3. Reaction intermediates and possible degradation pathway of MC-LR

The photocatalytic degradation pathways of MC-LR were investigated using NPT-EGC450 under visible light irradiation, and the reaction intermediates of MC-LR were detected by LC/MS. During the photocatalytic process, twenty-four intermediates (m/z = 481.3 (two intermediates), 520.3, 525.3 (two intermediates), 564.4, 569.3, 608.4, 613.3, 622.0 (two intermediates), 652.4, 657.4, 696.4, 734.5, 745.4, 795.4, 835.4 (two intermediates), 922.0, 1029.6 (two intermediates), 995.6 (two intermediates)) were detected and shown in Table S2 and Fig. S5. Among these, m/z 995.6 (two) are assigned to MC-LR molecules and their isomers, which are abundant initially and gradually decreased with extending reaction time. This indicates MC-LR was degraded during the photocatalytic process. The intermediates of m/z 1029.6, 835.4, and 795.4 have been reported in previous MC-LR photocatalytic degradation studies [3,4,34], suggesting the similar degradation pathways. Further degradation will be inferred based on other fragments.

According to the above intermediates, the proposed degradation pathways of MC-LR during the photocatalytic process are shown in Fig. 9. Under visible light irradiation, the isomer of MC-LR formed though the isomerization of the Adda moiety. According to previous studies [35,36], [tricycle-Adda^5]-MC-LR is considered as the isomer of MC-LR based on the differences in the retention time of two m/z 995.6 products. The products with m/z 1029.6 are assigned to the dihydroxylation of either C_4—C_5 or C_6—C_7 double bonds of the Adda side chain [37]. The dihydroxylated MC-LR underwent further oxidation to cleave at the diene structure, which is confirmed by the observation of cleavage products with m/z 835.4 (a type of ketone) and 795.4 (a type of aldehyde) [34]. The m/z 835.4 could also transform to the m/z 795.4 through oxidative cleavage at C_4—C_5 bond in residual Adda. The pathways of the Adda cleavage suggest the loss of toxicity of MC-LR during the photocatalytic process by the NPT-EGC composites [4]. Further reaction pathways leading to opening the peptide ring have been proposed and we observed the product with m/z 745.4 and 696.4 during the photocatalytic process, which can be rationalized *via* hydroxyl radical oxidation of the Mdha and Arginine. The 44 Da of difference in molecular weight is observed between the products of m/z 696.4, 652.4, 608.4

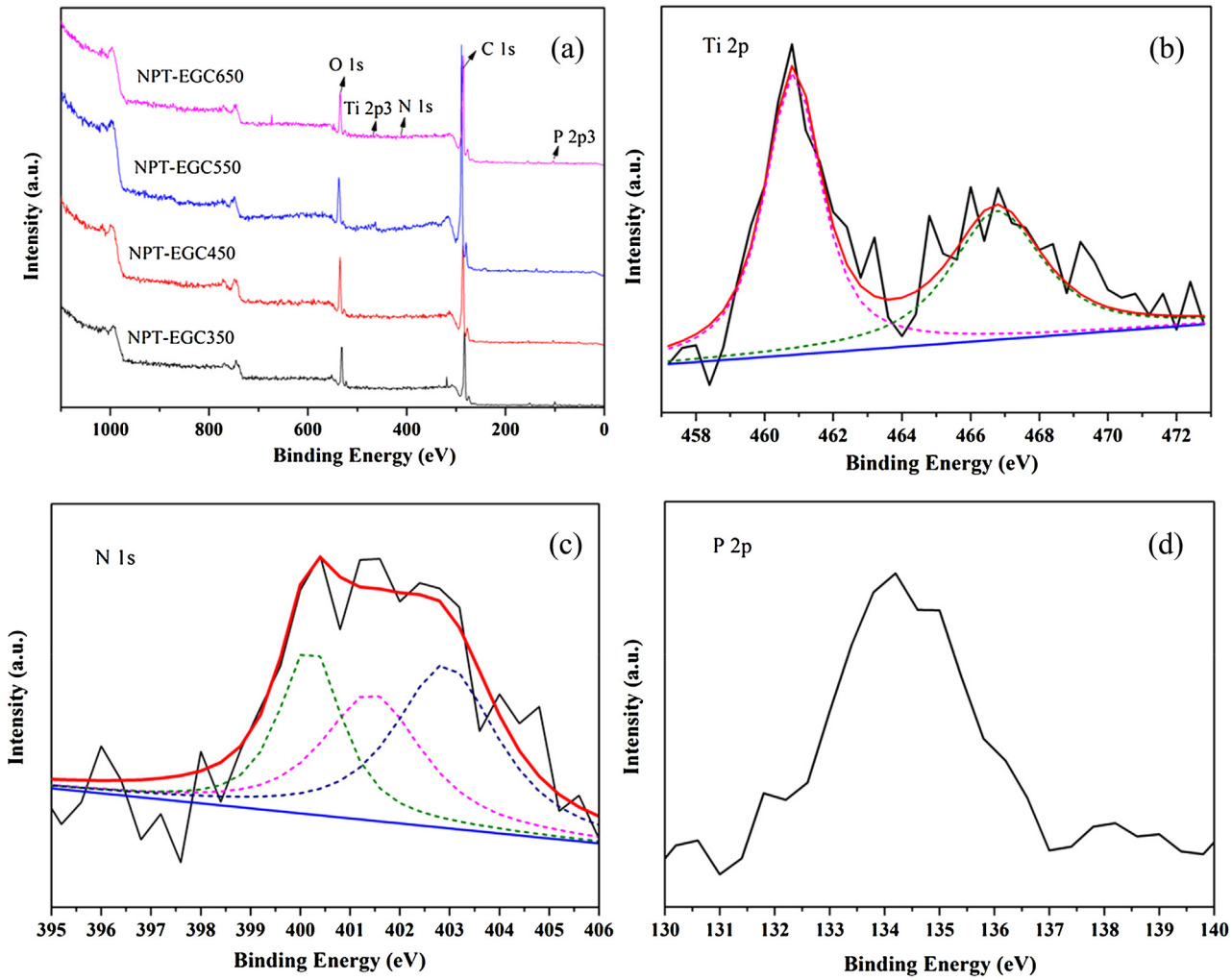

Fig. 6. XPS spectra of (a) NPT-EGC, (b) high resolution XPS of Ti 2p, (c) N 1s, and (d) P 2p of NPT-EGC450.

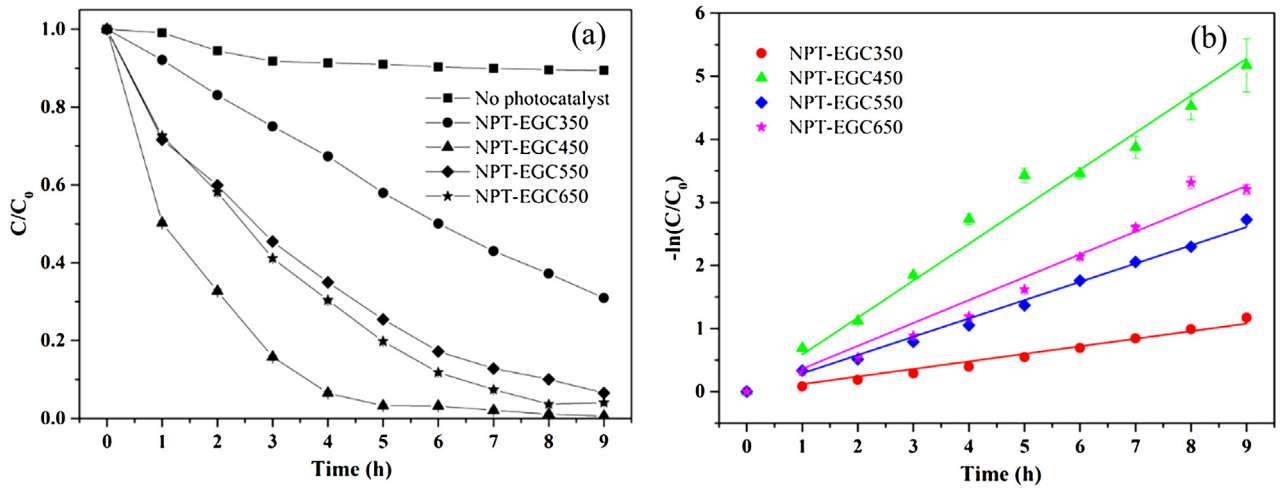

Fig. 7. Photocatalytic degradation of MC-LR by NPT-EGC shown by (a) Kinetics curves and (b) Langmuir-Hinshelwood kinetic fitting.

and 564.4, suggesting the gradual decarboxylation progress [38]. However, the decarboxylation pathways have not been observed in MC-LR reactions with ·OH as a result of the chemical insensitivity to the oxygen-centered free radicals for the free carboxyl groups in the polypeptide molecule [35]. This indicates photogenerated holes (h^+) should be responsible for the decarboxylation process in this study. Following these, the oxidation of the residual Adda, decarboxylation and deamination occurred with the detection of m/z 525.3 and 481.3. In general, the NPT-EGC photocatalyst can

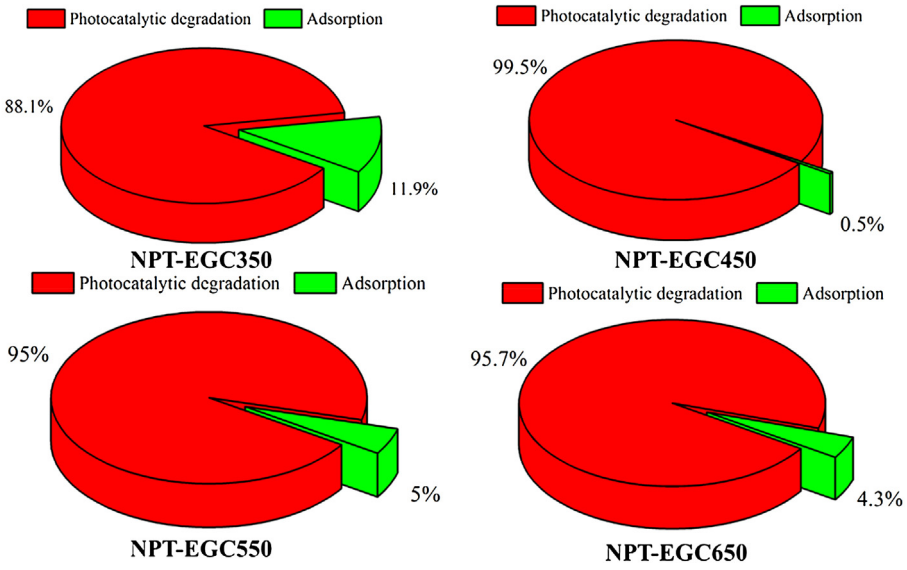

Fig. 8. Contribution of photocatalytic degradation and adsorption in the total removal of MC-LR.

destroy the Adda side chain and the peptide ring, thus breaking down MC-LR into small molecules under visible light irradiation.

3.4. Effect of environmental coexisting substances on photocatalytic degradation of MC-LR

In eutrophic waters, NO_3^--N and PO_4^{3-}-P are the predominant nutrients that result in eutrophication. Humic acid (HA) is the major part of natural organic matter (NOM) in waters where dead algal cells release MC-LR into waters, which is very common in MC-LR polluted water. These substances influence photocatalytic degradation of MC-LR and should be considered. In this study, we investigated the influence of these coexisting substances on the photocatalytic process based on their actual concentration in eutrophic waters. Before turning on the light, we conducted dark adsorption for 1 h in order to distinguish the influence of coexisting substances on adsorption and photocatalytic degradation. The results are shown in Fig. 10, and the parameters are listed in Table S3. Fig. 10 shows that the pre-adsorption rate decreases with the addition of coexisting substances. This observation is related to the surface interaction and competitive phenomena on adsorption; however, the influence of these coexisting substances is not limited to adsorption.

Fig. 10a shows the effect of NO_3^--N with the concentration of 0.1, 0.25 and 0.5 mg/L on MC-LR photocatalytic degradation. The pre-adsorption was inhibited after the addition of NO_3^--N but the pre-adsorption rate did not have obvious changes with the increase in NO_3^--N concentration. This implies that NO_3^--N may affect the solution conditions rather than compete surface adsorption sites. The total removal rate decreased from 93.9% to 77.4% while k_{app} value decreased from 0.41274 h^{-1} to 0.17419 h^{-1}.

Fig. 10b shows the effect of PO_4^{3-}-P with the concentration of 20, 40 and 60 μg/L on MC-LR photocatalytic degradation. When PO_4^{3-}-P was in a lower concentration (20 μg/L), the influence was focused on the photocatalytic reaction rate, and the total removal rate decreased to 85.3%. With the increase of PO_4^{3-}-P concentration, the pre-adsorption inhibition became obvious; meanwhile, k_{app} value decreased to 0.14380 h^{-1}. The total removal rate also significantly decreased to 67.2% as a result of the combined inhibition in adsorption and photocatalysis.

Fig. 10c shows the effect of HA with the concentration of 1, 2 and 5 mg/L on MC-LR photocatalytic degradation. HA has a more complicated influence mechanism. On the one hand, it is easily adsorbed on the photocatalyst surface, resulting in competitive adsorption and light shading. On the other hand, HA is an excellent natural photosensitizer and it can be excited by light irradiation and transfer electrons to the conduction band (CB) of a semiconductor, which could enhance the photocatalytic reaction [39]. When the HA concentration is 1 mg/L, the influence becomes focused on the competitive adsorption and adsorption induced photocatalytic inhibition. When the HA concentration increased to 2 mg/L, both the pre-adsorption rate and k_{app} value decreased greatly as a result of the combined influence of competitive adsorption and light shading. When the HA concentration comes to 5 mg/L, the photosensitization effect of HA began to be obvious, resulting in an increase of k_{app} value. It can be implied that the whole process influenced by HA is a balance of competitive adsorption and photosensitization.

Fig. 10d shows the effect of dead algal cells on MC-LR photocatalytic degradation. Dead algal cells' stock suspension, containing 1.885×10^7 cells/mL dead algal cells and 4.8 mg/L chlorophyll-*a* (chla), was prepared by repeating freeze-thawing in −20 °C. The stock suspension was diluted to get experimental concentration. The influence of dead algal cells mainly contains two aspects: the competitive adsorption of algal cells and the photosensitization of chla. When the cell concentration is in a low level (3.14×10^4 cells/mL), the competitive adsorption effect is not obvious. Chla can take in the visible light and produce electrons for photosensitization effect. When photosensitization began to play a more important role than competitive adsorption, the k_{app} value increased to 0.57231 h^{-1}. As cell concentration increased, competitive adsorption made a more serious inhibition effect, which resulted in the decrease of the k_{app} value. When the cell concentration came to 1.88×10^5 cells/mL, the k_{app} value decreased to 0.06622 h^{-1}.

3.5. Identification of reactive oxygen radicals and reusability

The reactive oxygen radicals in the photocatalytic process were identified by using radical scavenging techniques. In this study, several different scavengers, isopropanol (IPA), triethanolamine (TEA), and benzoquinone (BQ) were selected to quench •OH, h^+, and $\cdot O_2^-$ if formed during the photocatalytic process [40,41]. As shown in Fig. 11, the addition of IPA and TEA significantly quenched the pho-

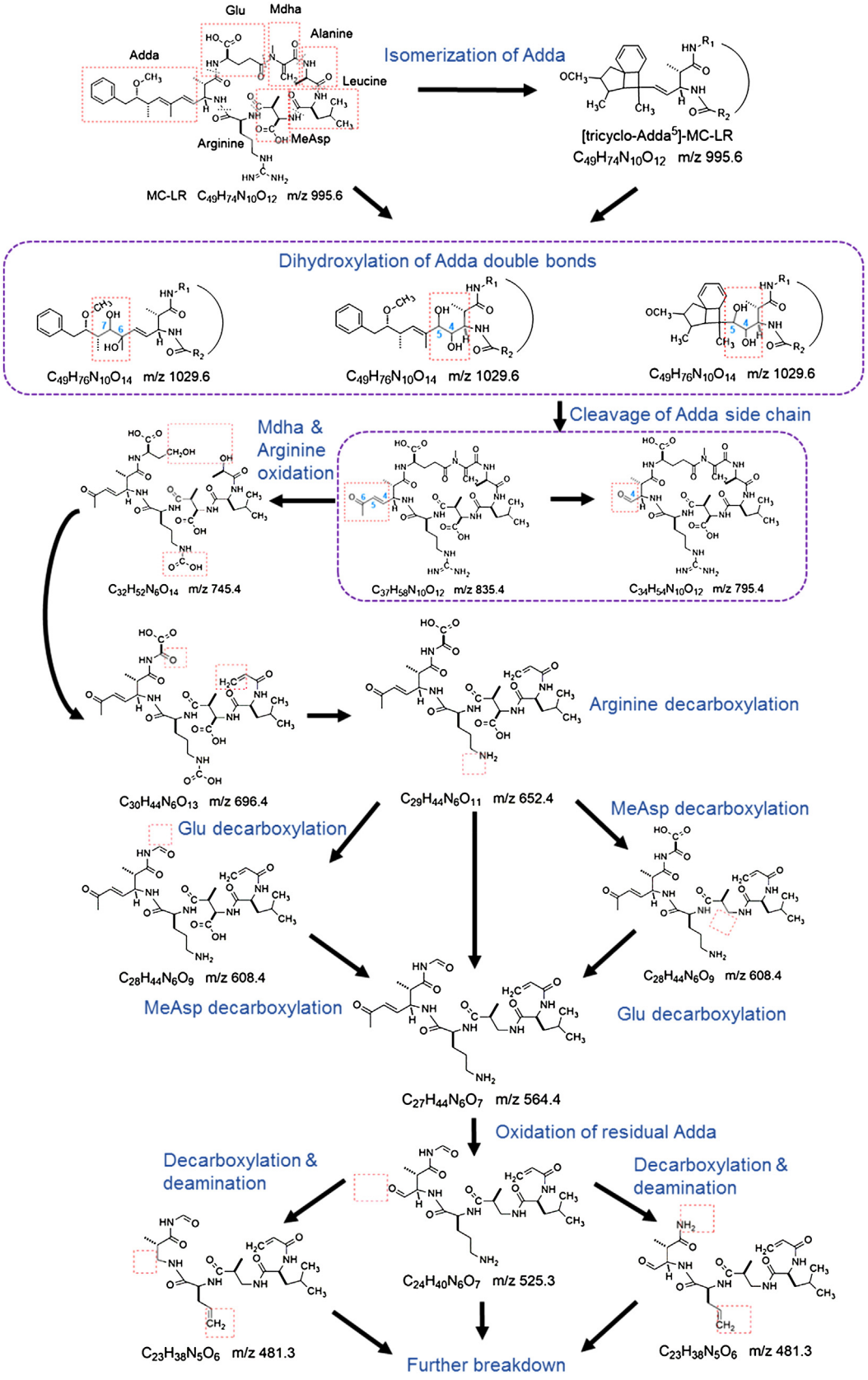

Fig. 9. The possible degradation pathway of MC-LR during the photocatalytic process.

tocatalytic process while the addition of BQ only slightly inhibited the photocatalytic degradation. This implied h^+ and •OH are the dominant reactive species responsible for the photocatalytic process. The reusability and stability of the photocatalyst are vital to the practical application. Recycling reactions were conducted to evaluate the reusability and stability of the floating photocatalyst.

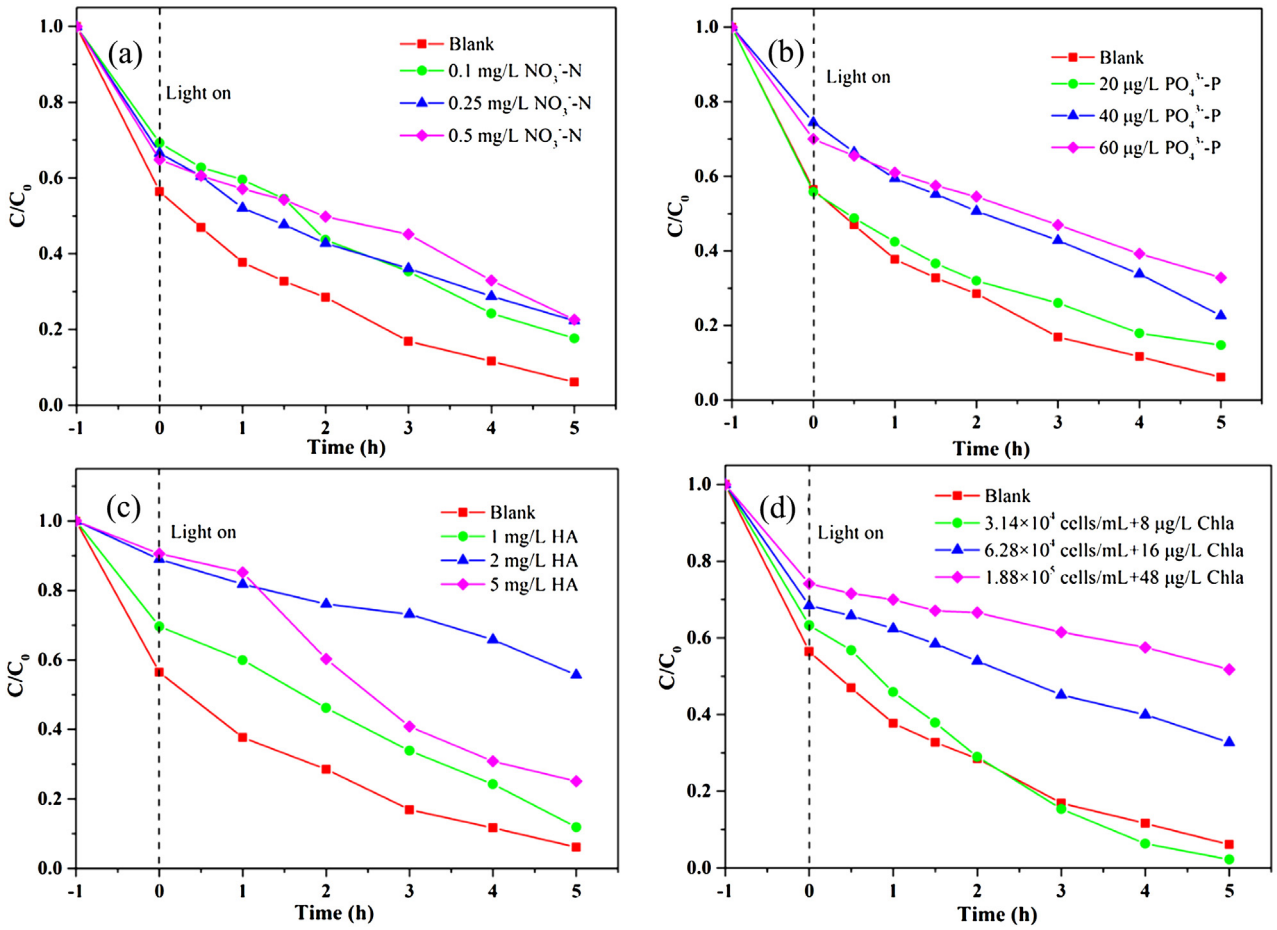

Fig. 10. Effect of coexisting substances on photocatalytic degradation of MC-LR by NPT-EGC450. (a) Effect of NO_3^--N; (b) effect of PO_4^{3-}-P; (c) effect of HA; (d) effect of dead algal cells.

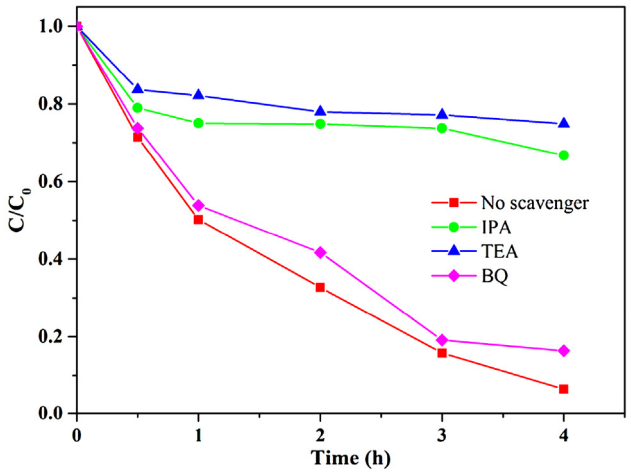

Fig. 11. MC-LR photocatalytic degradation by NPT-EGC450 under various scavengers.

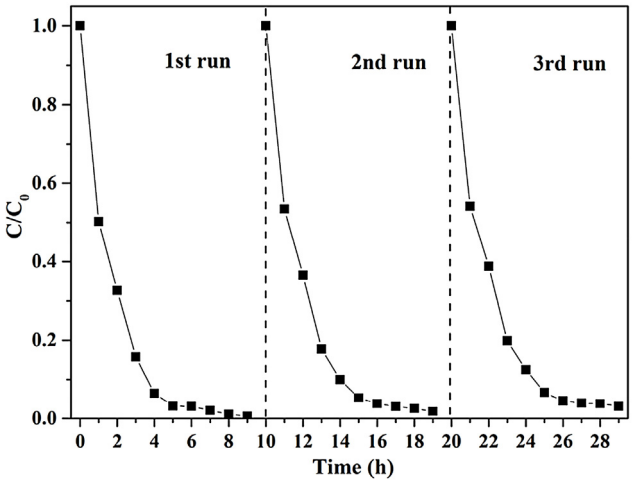

Fig. 12. Recycling properties of MC-LR removal by NPT-EGC450.

As shown in Fig. 12, after three consecutive cycles, the removal rates of MC-LR decreased from 99.4% to 96.8%, which indicates the high stability of the floating photocatalyst.

4. Conclusions

In this study, we synthesized N, P co-doped TiO_2/expanded graphite by carbon (NPT-EGC) floating composites for in situ photocatalytic degradation of MC-LR. According to the results from the characterization experiments, the NPT-EGC photocatalyst has a worm-like structure. The calcination temperatures can affect the forming of TiO_2 and carbon layer, resulting in the differences in specific surface area. Among the different NPT-EGC photocatalysts, NPT-EGC450 exhibited stronger photo-absorption and a lower recombination rate of the photo-generated charge carrier. Photocatalytic degradation experiments also showed NPT-EGC had

a higher removal rate of MC-LR (99.4%), thereinto photocatalytic degradation contributed 99.5% of total removal for NPT-EGC450. The toxic groups were destroyed during the photocatalytic process. Some coexisting substances (NO_3^--N, PO_4^{3-}-P, HA and dead algal cells) could affect the adsorption of MC-LR by NPT-EGC and inhibited photocatalytic degradation. After three consecutive cycles, the NPT-EGC photocatalyst could still retain good reusability and stability.

Acknowledgments

We gratefully acknowledge the support of this research by the National Natural Science Foundation of China (Award No. 21377095, 21277097) and the International Exchange Program for Graduate Students, Tongji University, Shanghai, China.

Appendix A. Supplementary data

Supplementary data associated with this article can be found, in the online version, at http://dx.doi.org/10.1016/j.apcatb.2017.01.046.

References

[1] L.X. Pinho, J. Azevedo, Â. Brito, A. Santos, P. Tamagnini, V.J.P. Vilar, V.M. Vasconcelos, R.A.R. Boaventura, Chem. Eng. J. 268 (2015) 144–152.
[2] M. Pelaez, B. Baruwati, R.S. Varma, R. Luque, D.D. Dionysiou, Chem. Commun. 49 (2013) 10118–10120.
[3] M.G. Antoniou, J.A. Shoemaker, A.A. de la Cruz, D.D. Dionysiou, Toxicon 51 (2008) 1103–1118.
[4] J. Andersen, C. Han, K. O'Shea, D.D. Dionysiou, Appl. Catal. B—Environ. 154–155 (2014) 259–266.
[5] S.M. El-Sheikh, G. Zhang, H.M. El-Hosainy, A.A. Ismail, K.E. O'Shea, P. Falaras, A.G. Kontos, D.D. Dionysiou, J. Hazard. Mater. 280 (2014) 723–733.
[6] L.A. Lawton, P.K. Robertson, B.J. Cornish, M. Jaspars, Environ. Sci. Technol. 33 (1999) 771–775.
[7] T. Fotiou, T.M. Triantis, T. Kaloudis, L.M. Pastrana-Martínez, V. Likodimos, P. Falaras, A.n.M. Silva, A. Hiskia, Ind. Eng. Chem. Res. 52 (2013) 13991–14000.
[8] R. Fagan, D.E. McCormack, D.D. Dionysiou, S.C. Pillai, Mater. Sci. Semicond. Process. 42 (2016) 2–14.
[9] M.J. Sampaio, C.G. Silva, A.M.T. Silva, L.M. Pastrana-Martínez, C. Han, S. Morales-Torres, J.L. Figueiredo, D.D. Dionysiou, J.L. Faria, Appl. Catal. B—Environ. 170–171 (2015) 74–82.
[10] Y. Liang, X. He, L. Chen, Y. Zhang, RSC Adv. 4 (2014) 56883–56891.
[11] R. Asahi, T. Morikawa, T. Ohwaki, K. Aoki, Y. Taga, Science 293 (2001) 269–271.
[12] G. Zhang, Y.C. Zhang, M. Nadagouda, C. Han, K. O'Shea, S.M. El-Sheikh, A.A. Ismail, D.D. Dionysiou, Appl. Catal. B—Environ. 144 (2014) 614–621.
[13] G. Liu, C. Han, M. Pelaez, D. Zhu, S. Liao, V. Likodimos, A.G. Kontos, P. Falaras, D.D. Dionysiou, J. Mol. Catal. A—Chem. 372 (2013) 58–65.
[14] T.M. Triantis, T. Fotiou, T. Kaloudis, A.G. Kontos, P. Falaras, D.D. Dionysiou, M. Pelaez, A. Hiskia, J. Hazard. Mater. 211–212 (2012) 196–202.
[15] M. Pelaez, P. Falaras, V. Likodimos, A.G. Kontos, A.A. de la Cruz, K. O'Shea, D.D. Dionysiou, Appl. Catal. B—Environ. 99 (2010) 378–387.
[16] M. Pelaez, A.A. de la Cruz, E. Stathatos, P. Falaras, D.D. Dionysiou, Catal. Today 144 (2009) 19–25.
[17] X. Wang, W. Wang, X. Wang, J. Zhang, Z. Gu, L. Zhou, J. Zhao, RSC Adv. 5 (2015) 41385–41392.
[18] P. Huo, Y. Yan, S. Li, H. Li, W. Huang, Desalination 256 (2010) 196–200.
[19] F. Magalhães, R.M. Lago, Sol. Energy 83 (2009) 1521–1526.
[20] L.C.R. Machado, C.B. Torchia, R.M. Lago, Catal. Commun. 7 (2006) 538–541.
[21] F. Yanfen, H. Yingping, Y. Jing, W. Pan, C. Genwei, Environ. Sci. Technol. 45 (2011) 1593–1600.
[22] F. Wei, L. Ni, P. Cui, J. Hazard. Mater. 156 (2008) 135–140.
[23] C. Ren, W. Qiu, H. Zhang, Z. He, Y. Chen, J. Mol. Catal. A—Chem. 398 (2015) 215–222.
[24] Y. Xia, Y. Jiang, F. Li, M. Xia, B. Xue, Y. Li, Appl. Surf. Sci. 289 (2014) 306–315.
[25] Q. Fang, M. Meier, J.J. Yu, Z.M. Wang, J.Y. Zhang, J.X. Wu, A. Kenyon, P. Hoffmann, I.W. Boyd, Mat. Sci. Eng. B—Adv. 105 (2003) 209–213.
[26] I. Iatsunskyi, M. Kempiński, G. Nowaczyk, M. Jancelewicz, M. Pavlenko, K. Załęski, S. Jurga, Appl. Surf. Sci. 347 (2015) 777–783.
[27] X. Li, P. Liu, Y. Mao, M. Xing, J. Zhang, Appl. Catal. B—Environ. 164 (2015) 352–359.
[28] K. Dai, L. Lu, C. Liang, Q. Liu, G. Zhu, Appl. Catal. B—Environ. 156–157 (2014) 331–340.
[29] C.-T. Hsieh, W.-S. Fan, W.-Y. Chen, J.-Y. Lin, Sep. Purif. Technol. 67 (2009) 312–318.
[30] G. Xue, H. Liu, Q. Chen, C. Hills, M. Tyrer, F. Innocent, J. Hazard. Mater. 186 (2011) 765–772.
[31] L. Xiong, W. Sun, Y. Yang, C. Chen, J. Ni, J. Colloid Interface Sci. 356 (2011) 211–216.
[32] X. Wang, X. Wang, J. Zhao, J. Chen, J. Zhang, J. Song, J. Huang, RSC Adv. 5 (2015) 66611–66620.
[33] S. Pavagadhi, A.L.L. Tang, M. Sathishkumar, K.P. Loh, R. Balasubramanian, Water Res. 47 (2013) 4621–4629.
[34] T. Fotiou, T.M. Triantis, T. Kaloudis, K.E. O'Shea, D.D. Dionysiou, A. Hiskia, Water Res. 90 (2016) 52–61.
[35] J. Chang, Z.-l. Chen, Z. Wang, J. Kang, Q. Chen, L. Yuan, J.-m. Shen, Chem. Eng. J. 276 (2015) 97–105.
[36] K. Kaya, T. Sano, Chem. Res. Toxicol. 11 (1998) 159–163.
[37] W. Song, A.A. De La Cruz, K. Rein, K.E. O'Shea, Environ. Sci. Technol. 40 (2006) 3941–3946.
[38] M.G. Antoniou, A.A. de la Cruz, D.D. Dionysiou, Environ. Sci. Technol. 44 (2010) 7238–7244.
[39] Y. Cho, W. Choi, J. Photochem. Photobiol. A 148 (2002) 129–135.
[40] Y. Ding, F. Yang, L. Zhu, N. Wang, H. Tang, Appl. Catal. B—Environ. 164 (2015) 151–158.
[41] W. Zhao, Y. Guo, Y. Faiz, W.-T. Yuan, C. Sun, S.-M. Wang, Y.-H. Deng, Y. Zhuang, Y. Li, X.-M. Wang, H. He, S.-G. Yang, Appl. Catal. B—Environ. 163 (2015) 288–297.